DOI:
10.1016/j.actbio.2019.10.043

Document Version
Publisher's PDF, also known as Version of record

Acta Biomaterialia 101 (2020) 168–182

Contents lists available at ScienceDirect

Acta Biomaterialia

journal homepage: www.elsevier.com/locate/actbio

Integration of biochemical and topographic cues for the formation and spatial distribution of invadosomes in nasopharyngeal epithelial cells

C.M. Tsang[a,b], Z.Y. Liu[c,d], W. Zhang[c,d], C. You[a], G.E. Jones[e], S.W. Tsao[a,*], S.W. Pang[c,d,**]

[a] School of Biomedical Sciences, LKS Faculty of Medicine, The University of Hong Kong, Hong Kong
[b] Department of Anatomical and Cellular Pathology, Faculty of Medicine, The Chinese University of Hong Kong, Hong Kong
[c] Department of Electrical Engineering and, Neuroscience, and Nanotechnology, City University of Hong Kong, Hong Kong
[d] Centre for Biosystems, Neuroscience, and Nanotechnology, City University of Hong Kong, Hong Kong
[e] Randall Centre for Cell and Molecular Biophysics, King's College London, London, UK

ARTICLE INFO

Article history:
Received 26 April 2019
Revised 16 October 2019
Accepted 30 October 2019
Available online 2 November 2019

Keywords:
Invadosomes
Nasopharyngeal Carcinoma (NPC)
Engineered platform
Topographical Pattern
Biomimetic system

ABSTRACT

Invadosomes are invasive protrusions generated by cells which can secrete matrix metalloproteinases for focal digestion of extracellular matrix. They also aid invasive cancer cells in their transmigration through vascular endothelium. However, how the physical and chemical cues in a three-dimensional (3D) system signal the spatial localization of invadosomes remains largely unknown. Here we study the topographic guidance of invadosome formation in invasive nasopharyngeal cells under the stimulation of an inflammatory cytokine, TGF-β1, using engineered gratings with different width and depth. We first report that TGF-β1 can act as an external signal to upregulate the formation of invadosomes with a random distribution on a plane 2D surface. When the cells were seeded on parallel 3D gratings of 5 µm width and 1 µm depth, most of the invadosomes aligned to the edges of the gratings, indicating a topographic cue to the control of invadosome localization. While the number of invadosomes per cell were not upregulated when the cells were seeded on 3D topography, guidance of invadosomes localization to edges is correlated with cell migration directionality on 1 µm deep gratings. Invadosomes preferentially form at edges when the cells move at a lower speed and are guided along narrow gratings. The invadosomes forming at 3D edges also have a longer half-life than those forming on a plane surface. These data suggest that there are integrated biochemical and 3D geometric cues underlying the spatial regulation of invasive structures so as to elicit efficient invasion or metastasis of cells.

Statement of significance

Nasopharyngeal cells were integrated with the biological cues and matrix topography to govern the activity and spatial distribution of invadosomes. The biochemical induction of invadosome formation by TGF-β1 in nasopharyngeal cells was observed. When the cells were seeded on parallel 3D gratings, most of the invadosomes aligned to the edges of the gratings due to topographical induced invadosome localization. While the number of invadosomes per cell were not upregulated, guidance of invadosomes localization to edges is correlated with cell migration directionality on 1 µm deep gratings. Invadosomes preferentially form at edges with a higher stability when the cells are guided along narrow gratings. The integrated biochemical and 3D geometric cues could elicit efficient invasion or metastasis of cells.

1. Introduction

Invadosomes are matrix metalloproteinase (MMP)-secretory microdomains that can focally interact with and digest the extracellular matrix (ECM) [1]. They can be observed in both normal and cancer cells and in different conformations, such as aggregates, individual dots, rosettes or linear structures [2]. These degradative

* Corresponding author.
** Corresponding author at: Department of Electrical Engineering, City University of Hong Kong, Hong Kong.
E-mail addresses: gswtsao@hku.hk (S.W. Tsao), pang@cityu.edu.hk (S.W. Pang).

https://doi.org/10.1016/j.actbio.2019.10.043

structures are important for many physiological purposes including trafficking of immune cells or bone reabsorption. However, it has been suggested that cancer cells may hijack this invasive machinery for cancer invasion during long term interaction with an inflammatory environment [3]. Especially in metastatic cells, it has been postulated that invadosome is utilized as an invasive device for penetrating extracellular matrix and blood vessel endothelium layer to invade a new tissue site for growth [4–6].

Nasopharyngeal carcinoma (NPC) is one of the most common malignancies in southern China and Southeast Asia [7–9]. It is a highly invasive and metastatic cancer. Most patients present with locally advanced stage or with distant metastasis into other organs, such as bones, lungs, liver and distant lymph nodes. While primary NPC tumors are known to have high response rate to chemoradiotherapy, metastatic recurrence accounts for most of the patients' death [7,10]. Therefore, detailed elucidation of the invasive mechanisms mediated by invadosomes in NPC is of urgent need for devising feasible therapeutic strategies to suppress the metastatic spread of the cancer cells.

The basic unit of an invadosome consists of an F-actin core surrounded by adhesive molecules and a range of actin-regulating proteins, including kinase signaling molecules, cortactin, neural Wiskott–Aldrich syndrome protein (N-WASP) and Arp2/3 [4,11]. Various signaling pathways have been shown to be involved in regulating the formation of invadosomes, resulting in actin assembly to mature structures that release MMPs to focally degrade the ECM [3]. In addition, invadosomes are also reported to be required in intravasation and extravasation of cancer cells through the vascular systems [5,6]. Interestingly a previous report showed that invadosomes form at the Y-junctions of adhesive endothelial cells to facilitate ingression of cancer cells into the blood vessels [6], indicating the cells may be able to sense local topological features of endothelial cell junctions that guide the invadosomes to localize at such junctions.

Despite many studies on the role of invadosomes in tumor cell invasion and metastasis, the modulation of the generation and stability of invadosomes in nasopharyngeal cells under stimulation from the inflammatory stroma remain largely undefined. Development of NPC is known to be related to inflammatory status of the nasopharynx. NPC tissues are also highly infiltrated by tumor associated macrophages and lymphocytes, which are rich sources of TGF-β1 [12]. It has been reported that TGF-β1 level is higher in serum of NPC patients than healthy individuals [13]. TGF-β1 has been reported to upregulate invadosome formation in other cell types including breast cancer cells [14,15] and endothelial cells [16]. In this study, we describe efforts to understand the induction effect of TGF-β1 in generating invadosomes by nasopharyngeal cells. Additionally, we aim to understand how the nasopharyngeal cells react to physical signals such as substrate topography and rigidity [3,17]. How they integrate all these biochemical and physical signals remains elusive. There are only a few studies describing the very existence and role of invadosomes *in vivo* [5,6,18–20]. In addition, most studies on invadosome generation use cells seeded on plane substrates which can only represent a minority of *in vivo* situations. There is a pressing need to understand the additional complexity imposed by the three-dimensional (3D) topography in governing invasive cell behavior.

Advances in nanotechnology now allow a closer mimicry of the *in vivo* 3D interactions of cells [17]. With designed topographies or stiffness of substrates, we have previously reported that cell migration speed and directionality could be regulated by influencing the formation of filopodia and focal adhesions (FAs) [21,22]. We hypothesize that the formation of invadosomes as ventral membrane protrusions in invasive cells is also affected by the physical and chemical microenvironment of the ECM. In addition, how the invasive nasopharyngeal cells probe the 3D environment and determine where to form matrix-degradative invadosomes remains unknown. Despite other studies having reported the topographic guidance of invadosomes in other cell types such as dendritic cells [23], the cellular context may impose a different mechanism in regulating the formation of invadosomes, which are adapted for their physiological functions in the stroma [24]. The goal of this study was to evaluate how the nasopharyngeal cells integrate the biological cues and matrix topography to govern the activity and spatial distribution of invadosomes.

2. Materials and methods

2.1. Cell culture

Three premalignant nasopharyngeal cell lines (NP361hTert, NP460hTert, and NP550hTert) and one cancerous nasopharyngeal cell line (NPC43) were used in this study. The premalignant cell lines were obtained by transduction of the human telomerase reverse transcriptase (hTert) gene into primary cultures of tumor-adjacent premalignant nasopharyngeal tissues. NPC43 is a newly established NPC cell line which has been characterized extensively and reported in a recent study [25]. The culture conditions of primary and immortalized NPE cells have been published previously [26]. Briefly, NP361hTert, NP460hTert, and NP550hTert were maintained in serum-free culture medium made up of a 1:1 mixture of Defined Keratinocyte-SFM (Gibco) and EpiLife medium (Cascade Biologics) with the addition of growth supplements provided by the manufacturers. NPC43 cells were cultured in RPMI medium 1640 (1X, Gibco) supplemented with 10% fetal bovine serum (FBS), 1% antibiotic antimycotic (Gibco; 100 units/ml penicillin G sodium, 100 mg/ml of streptomycin, and 0.25 mg/ml of amphotericin B), and 0.2% 2 mM rock inhibitor Y-27,632 (ENZO). The cells were incubated at 37 °C in a 5% CO_2 incubator and the medium was changed every two days.

2.2. Invadosome formation and degradation assay

The 12-mm circular glass coverslips at the bottom of culture dishes were coated with 100 µl of 25 mg/ml FITC-gelatin and then cross-linked with 0.5% glutaraldehyde for 15 min at room temperature. After washing with PBS for three times, the coverslips were treated with 5 mg/ml sodium borohydrate for 5 min to quench autofluorescence of residual glutaraldehyde. The coated dishes were then sterilized with 70% ethanol. Either control or TGF-β1 (2 ng/ml for 24 h) treated nasopharyngeal cells were then cultured in the gelatin-coated dishes for 3–9 h. Cells were fixed in 4% paraformaldehyde for 15 min and permeabilized with 0.1% Triton X-100 for 5 min. After blocking in 1% BSA for 30 min, the cells were incubated with fluorophore-conjugated phalloidin (Invitrogen) for 10 h. Samples were observed with a confocal microscope (LSM780, Carl Zeiss). The percentage of cells with invadosomes and the number of invadosomes per cells were counted manually from the microscopy images. When counting for the number of invadosome, each punctate dot of actin with a black hole underneath was counted as one invadosome. To quantitate the gelatin degradation activity of invadosomes, the degradation area and the cell area were analysed with the ImageJ software. More than 10 randomly selected fields containing more than 100 cells in total, were imaged with a 40 × objective and analyzed for each experiment.

2.3. Generation of LifeAct-expressing cells for live-cell imaging

LifeAct-Cherry and LifeAct-GFP constructs were a kind gift from Dr Michael Way (The Francis Crick Institute [27]). They are generated by linker cloning LifeAct into a pLVX-Cherry/GFP-puro vector.

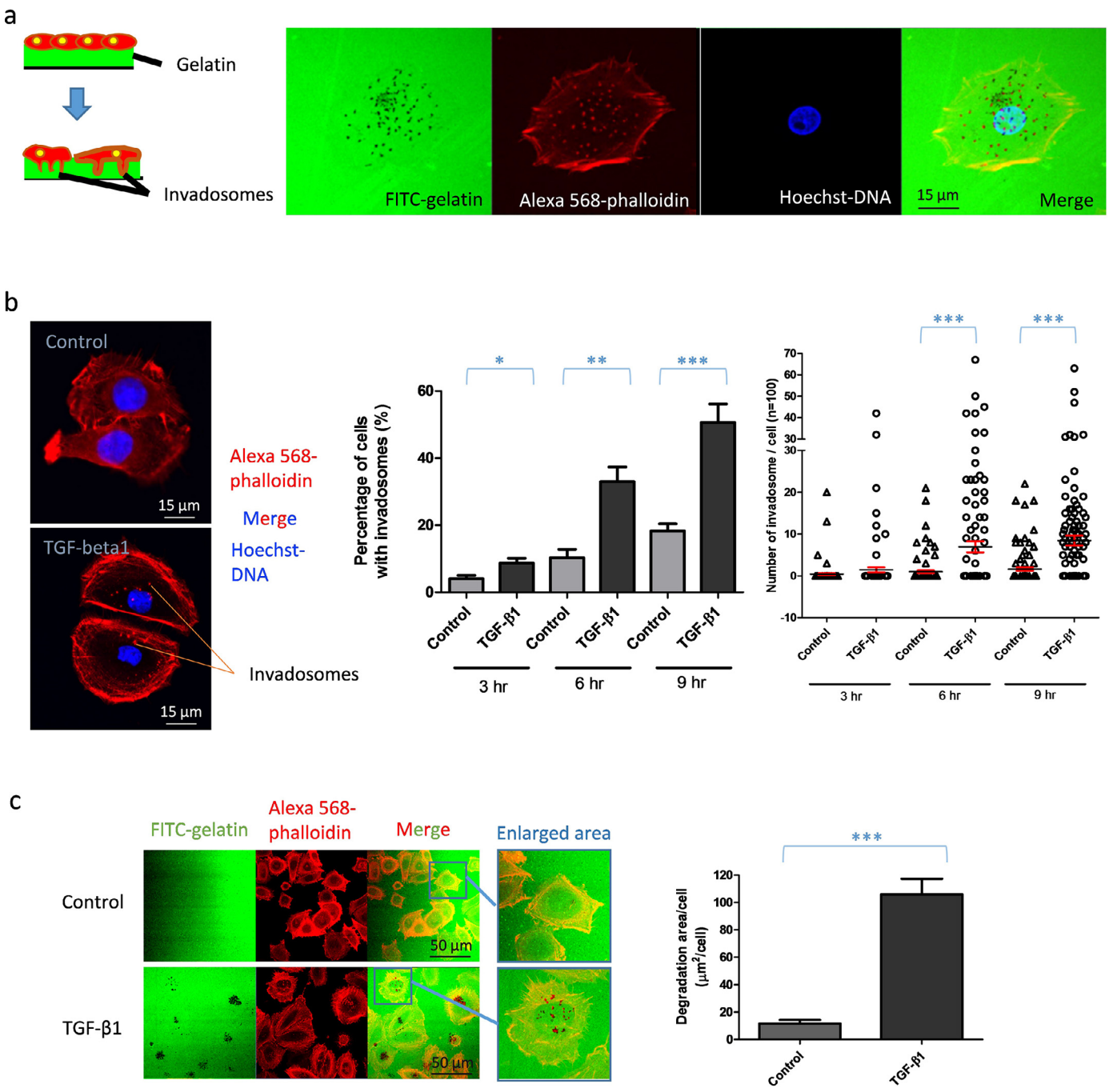

Fig. 1. TGF-βbeta1 upregulated the formation of invadosomes and gelatin degradation in nasopharyngeal cell line, NP460hTert. (a) Left panel: The generation of protrusive invadosomes from cells seeding on gelatin. Right panel: Confocal images showing the actin-rich invadosomes appear as punctate dots (stained by Alexa568-phallodin) and are co-localized with the areas of degraded gelatin (black holes on FITC-conjugated gelatin). (b) Left panel: Confocal images showing the increase of invadosomes in TGF-β1-treated cells compared to control cells. Middle panel: Bar chart showing the treatment of TGF-β1 upregulated the percentage of cells in forming invadosomes in a time-dependent manner ($n = 100$). Right panel: Dot plots showing the number of invadosomes per cell was upregulated by TGF-β1 ($n = 100$). (c) TGF-β1 enhanced the gelatin degradation of cells as indicated by the representative images (left panel) and analysed by imaging software of more than 10 random fields (right panel). (d) Live-cell imaging of an invadosome-forming NP460hTert cell under the treatment of TGF-β1. $^{*}p < 0.05$, $^{**}p < 0.005$ and $^{***}p < 0.0005$.

Lentiviruses production and infection were performed. Stable expression of LifeAct in nasopharyngeal cell lines were selected by 1 μg/ml puromycin.

2.4. Fabrication technology for engineered platforms

Engineered platforms with gratings of different depth, width, and stiffness were designed and fabricated. Besides forming the 2D patterns with different grating dimensions, the height of the gratings was also varied from 0.1 to 1 μm deep. This allowed the cells to contact not only the top 2D surface, but also the grating sidewalls with different heights and the bottom surface in between the gratings. As cells could experience the top surface, the sidewalls, and the bottom surface in the engineered platforms, they functioned as 3D substrates for cell migration. The PDMS grating platforms were fabricated by replicating silicon (Si) molds [22]. Silicon molds with gratings were formed by photolithography and reactive ion etching. A self-assembled anti-stiction layer was formed

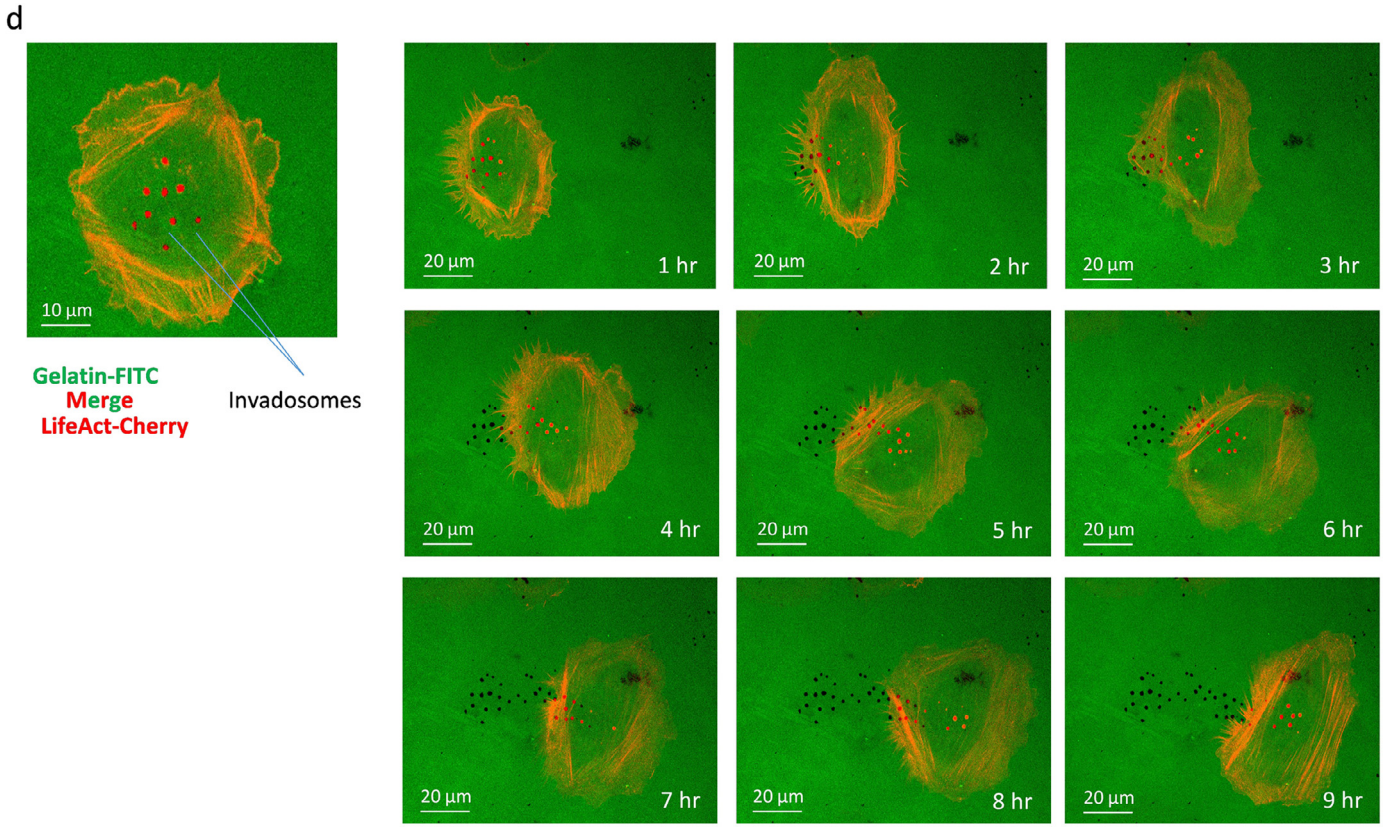

Fig. 1. Continued

by coating trichloro(1H,1H,2H,2H-perfluorooctyl) silane (FOTS) on the Si mold. To replicate the patterns on the Si mold, a PDMS layer was spin-coated on the mold, baked at 80 °C for 6 h, and separated from the mold by peeling. In order to form a hydrophilic surface for cell seeding, the PDMS platforms were treated in an O_2 plasma using 20 sccm O_2 at 80 mTorr and 60 W RF power for 1 min. The contact angle of water droplet on the PDMS platforms before and after the O_2 plasma treatment was 116°±2° and 10°±5°, respectively. The plasma-treated PDMS platforms were immediately stored in deionized (DI) water to maintain the hydrophilicity.

2.5. Time-lapse imaging

The engineered platforms were bonded on 35 mm diameter glass bottom confocal dishes after an O_2 plasma treatment for 1 min with a flow rate of 20 sccm O_2, chamber pressure of 80 mTorr, and RF power of 60 W. The cells were seeded at a density of 6×10^4 cells per cm^2 onto the platforms and incubated for 6 h at 37 °C in 5% CO_2 inside a humidified incubator. After the incubation, the medium was replaced by the 1:1 mixture of the cell culture medium and CO_2-independent medium (Invitrogen 18,045–088) supplemented with 10% FBS, antibiotic antimycotic (100 units/ml of penicillin, 100 mg/ml of streptomycin, and 0.25 mg/ml of amphotericin B), and 2 mM alanyl-L-glutamine. The cells were imaged under an upright microscope (Nikon Eclipse Ni-U or Carl Zeiss LSM800) equipped with an incubation chamber at 37 °C. Images were captured every 5–10 min up to a period of 15 h. Digital images were converted to video using Zen software (Zeiss).

2.6. Analysis of cell movement

NIH ImageJ (Version 1.50i) software package with manual tracking plugin was used to analyze the cell migration characteristics. Cells that divided or contacted with other cells during the 15 h imaging period were not included in the analysis. The cell migration speed and directionality were calculated from these images. Statistical difference between groups was tested using the one-way ANOVA with significant level at $p < 0.05$. All the results were presented as mean ±standard error of the mean (SEM). Migration direction angle was obtained by calculating the average angle between cell migration direction and grating orientation. A migration direction angle of 45° represented random migration without orientation on the platforms, while smaller angles indicated more directional migration of NPC43 cells along the gratings. Fitting cell shape to an ellipse, aspect ratio of NPC43 cells was calculated by taking the ratio of long axis *versus* short axis of the ellipse. Aspect ratio of 1 meant rounded cell shape, while smaller than 1 showed elongated shape.

2.7. Statistical analysis

Graphs and statistics were compiled using Prism (Graphpad software). Comparison of two data sets was carried out using a Student's *t*-test. Comparison of more than two data set was performed with one-way ANOVA using multiple comparison analysis. $p<0.05$, $p<0.05$ and $p<0.005$ is represented by single, double and triple asterisks, respectively.

3. Results

3.1. TGF-β1 promotes the formation of invadosomes in multiple nasopharyngeal cell lines

Control of cell invasion is important in numerous key biological processes and is implicated in pathological development of

metastasis [28]. Potential *in vivo* stimuli including cytokines secreted from inflammatory stromal cells, and ECM topography and stiffness on the dynamic assembly of invadosomes are still not well understood. In this study, we first sought to elucidate if TGF-β1, an inflammatory cytokine present at high level in NPC patients [13], had any effect on the formation of invadosomes in nasopharyngeal cells. We first assessed the formation of invadosomes of a premalignant nasopharyngeal epithelial cell line, NP460hTert, using conventional two-dimensional (2D) surfaces coated with FITC-gelatin (Fig. 1a). The actin-rich invadosomes were visualized as F-actin punctate dots after staining with phalloidin. Invadosomes were present on the ventral surface and digested the gelatin, leaving some black holes on the FITC-gelatin coated surface (Fig. 1a). Under the treatment of TGF-β1 the percentage of cells that could form invadosomes and number of invadosomes per cell significantly increased in a time-dependent manner (Fig. 1b). In the control group, there were only around 5–20% of cells forming invadosomes, as indicated in the bar chart in Fig. 1b. The image panel of the control cells shows the ones without any invadosomes. Notably, the highest number of invadosomes that could form in an invadosome-positive cell increased from ~20 to ~70 between control and TGF-β1-treated cells. Moreover, TGF-β1 also promoted the degradation of gelatin by invadosomes (Fig. 1c). We have also stably expressed the F-actin-binding peptide LifeAct, in nasopharyngeal NP460hTert cells to allow live-cell imaging of invadosome formation and gelatin digestion under the activation of TGF-β1 (Fig. 1d, and Supplementary video SV1).

To further confirm that TGF-β1promoted the formation of invadosomes in nasopharyngeal cells, we extended the invadosome assay to more premalignant and cancerous nasopharyngeal cell lines (Fig. 2). The percentage of invadosome-forming cells, the number of invadosomes per cells and gelatin degradation ability were all significantly upregulated in TGF-β1-treated cells compared to control cells (Fig. 2a–c). To further validate the induction of invadosome formation by TGF-β1 in nasopharyngeal cells, invadosome assay was performed on nasopharyngeal cells stably expressing wildtype or dominant-negative TGF-β1 receptor (Fig. 2d) post 36 h of TGF-β1 treatment. TGF-β1-mediated gelatin degradation was abolished in the cells with the dominant functional defective TGF-β1 receptor. We therefore conclude that TGF-β1 enhances the formation of invadosomes in nasopharyngeal epithelial and cancerous cells.

3.2. Invadosomes preferentially form at the edges of ridges

We have demonstrated above that TGF-β1 is a stimulator of invadosome formation in nasopharyngeal cells cultured on two-dimensional (2D) surfaces. However, in *in vivo* conditions cells encounter 3D extracellular surfaces. We therefore studied how the 3D topography would affect the formation of invadosomes in nasopharyngeal cells, and if this would modulate the induction effect of TGF-β1. Engineered platforms with gratings of different depth, width, and stiffness were designed and fabricated to study the effects of the platforms on cell migration behavior as shown in Fig. 3a–c. Figs. 3b shows micrographs for platforms with grating depth varied from 0.1 to 1 µm with 5 µm width and 5 µm space (as shown in Fig. 3c) and with PDMS base:agent mix ratio of 10:1 (as shown in Fig. 3d). Fig. 3c shows grating width varied from 5 to 50 µm with 1 µm depth. The grating width was varied from 5, 18, to 50 µm because the designs provided trench dimensions that were smaller than, similar to, and larger than the cell size of ~20 µm. The platform stiffness was varied by adjusting the polydimethylsiloxane (PDMS) base:agent mix ratio from 5:1 to 30:1. Young's modulus of PDMS with different mix ratios was measured by a nanoindenter, and the results are shown in Fig. 3d. Young's modulus of PDMS with higher mix ratio (30:1) was approximately 1.1 MPa. This parameter increased to 5.0 and 7.3 MPa with mix ratio of 10:1 and 5:1, respectively. Therefore, PDMS platforms were stiffer with lower mix ratio. The thin film of gelatin is for indicating the degradative properties of the invadosomes. An invadosome is presumably an invasive structure, which can localize the secretion of MMP and digest the gelatin. The gelatin coating on the surface, no matter on plane or grated surfaces, is very thin and only around 50 nm thick. The depths (*e.g.* 0.1, 0.25, 0.5 and 1 µm) of the PDMS-ridges were chosen according to the topology of ECM bundles within the tissue, as they vary in size between 30 and 300 nm.

After seeding TGF-β1-treated cells on the parallel 5 µm wide 3D gratings, most of the invadosomes aligned at the edges of the gratings (Fig. 3e). Similar effects were observed when the cells were seeded on 3D triangular pattern (Supplementary Figure S1). These suggest that the spatial distribution of invadosomes changed from a random distribution on 2D plane surface to a guided distribution to 3D edges. To further confirm there was a directed formation of invadosomes at the edges of ridges, we measured invadosome formation simultaneously on a plane surface and on gratings using live-cell imaging (Fig. 3f, and supplementary video SV2). The nearest neighbor angles were calculated according to the schematic diagram in Fig. 3g. Perfect alignment of invadosomes on a linear edge would show a nearest neighbor angle (NNA) of 90° to each other. We found that the parallel gratings induced a polarization of NNA near to 90° between adjoining invadosomes (Fig. 3h). On the other hand, the invadosomes of cells seeded on 2D surfaces had a random distribution of NNA to each other. In this experiment, the invadosomes were shown to preferentially align to the edges of the 1 µm deep grating, which may resemble the *in vivo* 3D patterns introduced by ECM bundles or Y-gaps between endothelial cells often used for transmigration of invasive cells. Most invadosomes did not form on the top ridges due to their preferential formation along the edges of gratings with steps. The steps are related to the grating depths with sidewalls and they provide larger cell contact area. Moreover, cells have to curve around the steps, which could trigger the invadosome formation. Some invadosomes, but with lower number, still formed on top of the gratings.

In assessing the active formation of invadosome, the cells are seeding on a surface with a pre-coated and thin layer of gelatin, thereby the degradation of gelatin is a good indicator for a functional invadosome. To indicate the actin core structures aligning to the ridges' edges are functional invadosomes, we have coated the gratings with FITC-conjugated gelatin and stained the cells with Alexa568-conjugated phalloidin to visualize the actin-rich invadosomes (Supplementary Figure S2). The actin cores were shown to be co-localized with the black holes, suggesting the invadosomes could focally digest the gelatin along the edges. The generation of actin cores on the edges of ridges is highly associated with subsequent degradation of gelatin, when the cells were seeded on FITC-coated gelatin.

3.3. 3D topography did not act as a stimulatory signal for invadosome formation

Next we aimed to discover if the 3D grating itself would serve as an induction or a suppression signal for invadosome formation. Control and TGF-β1-treated cells were seeded on both plane and grated surfaces and counts taken of the percentage of invadosome-forming cells. The percentage of invadosome-positive cells remained similar on plane or grated surface (Fig. 4a). Moreover, the number of invadosomes was also not significantly altered in either control or TGF-β1-stimulated cells when seeded on plane or grated surfaces (Fig. 4b). Thus the grating by itself did not affect the biological induction of TGF-β1 in forming invadosomes. The number of invadosomes were also comparable on control and

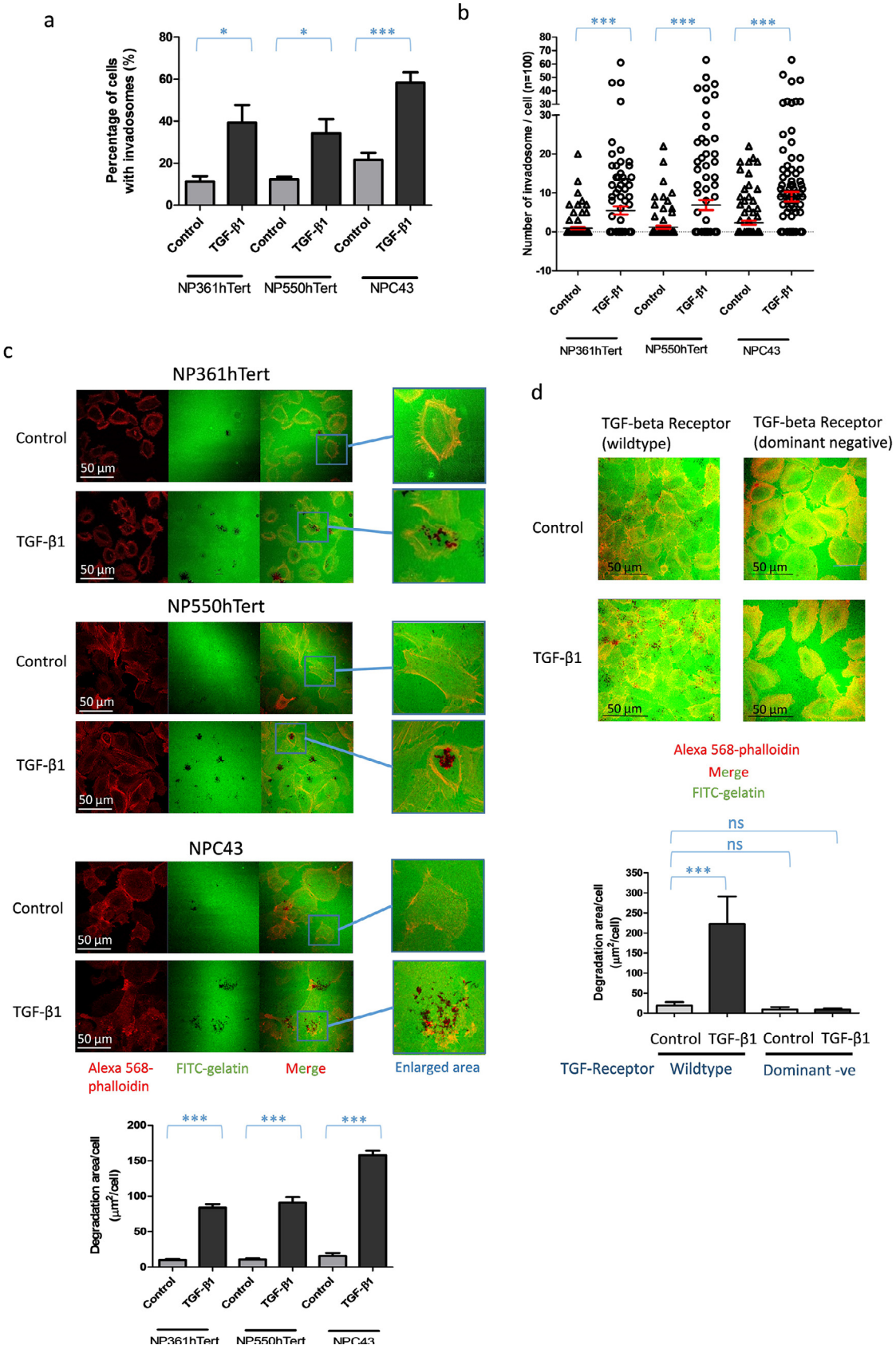

Fig. 2. Formation of invadosomes and gelatin degradation were upregulated by TGF-β1 in multiple nasopharyngeal cell lines (NP361hTert and NP550hTert) and NPC cell line (NPC43). TGF-β1 upregulated (a) the percentage of cells forming invadosomes, (b) the number of invadosomes per cell and (c) the degradative properties of all the tested nasopharyngeal cell lines. (d) Blockage of TGF-β1 signaling by stable expression of non-functional TGF-β-receptor abolished the degradation of gelatin by invadosomes in cells treated with TGF-β1. $^{*}p < 0.05$, $^{***}p < 0.0005$ and ns: no significance.

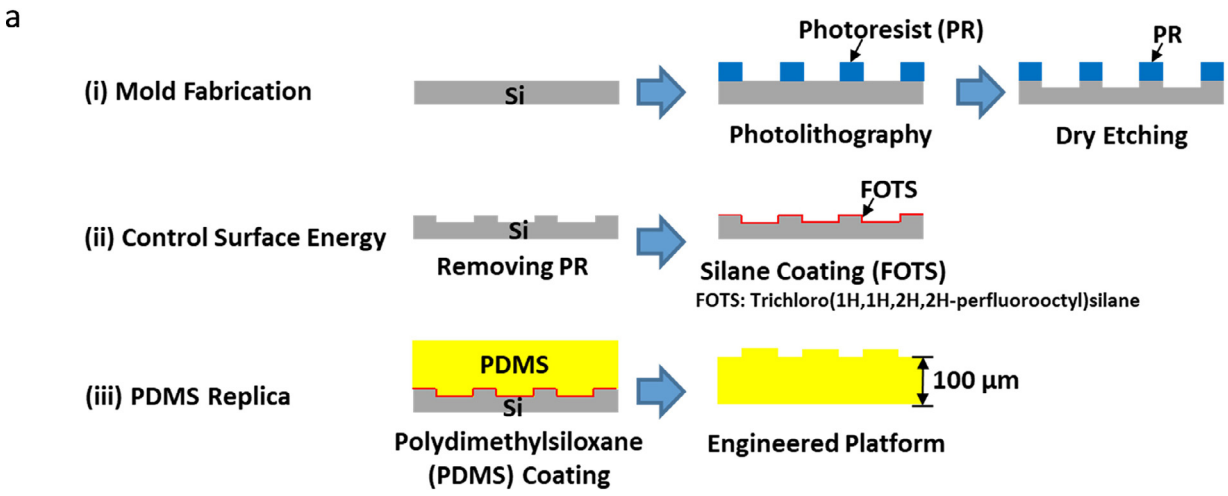

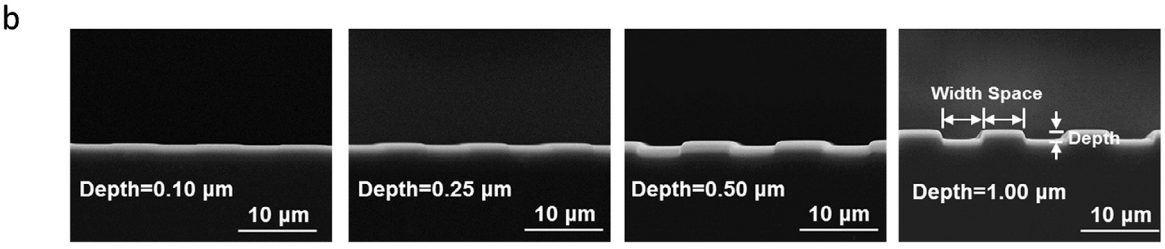

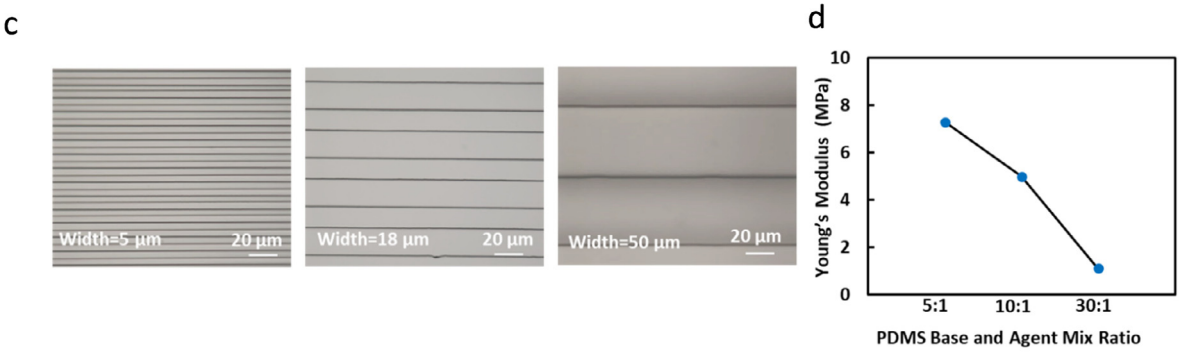

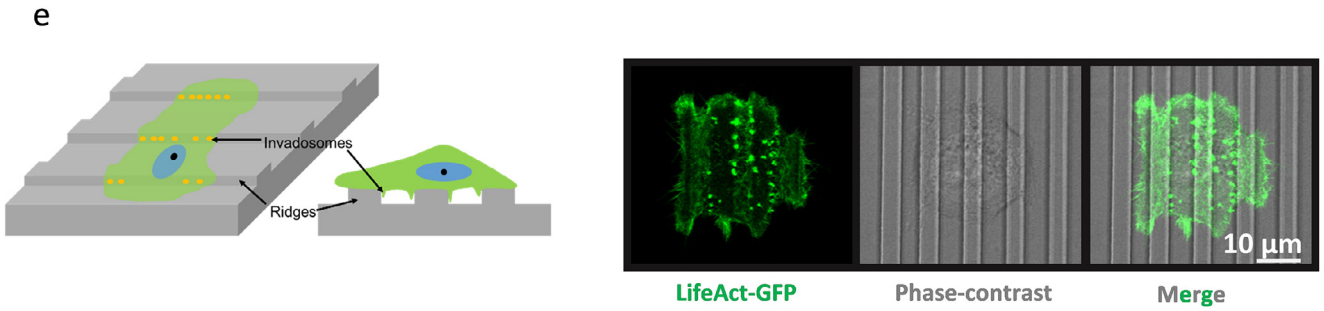

Fig. 3. Alignment of invadosomes at the edges of 3D gratings. (a) Fabrication process of engineered platforms with various grating width, depth, and stiffness. (b) Grating with different depth of 0.10, 0.25, 0.50, and 1.00 µm. (c) Optical micrographs of grated platforms with width/space of 5/5 µm, 18/18 µm, and 50/50 µm with depth of 1.00 µm. (d) Young's modulus dependence on PDMS base:agent mix ratio for grating width/space of 5/5 µm and depth of 1.00 µm (Error bar ±12 kPa). (e) Guided formation of invadosomes at the edge of parallel gratings as demonstrated in schematic cartoon [left panel] and representative confocal image [right panel]. (f) Live-cell imaging showing the formation of invadosomes in cells seeded on plane or grated surface. (g) Nearest neighbour angles (NNA, θ) were determined by calculating the angle of the nearest neighbour invadosome with respect to the y-axis. The green dots represent invadosomes. The blue dotted line outlines a putative cell boundary. (h) The NNA of invadosomes reveals the alignment of invadosomes on the edges of 3D patterns. The 5 µm 3D gratings induced a polarization of the NNA towards 90° ($n = 100$).

f

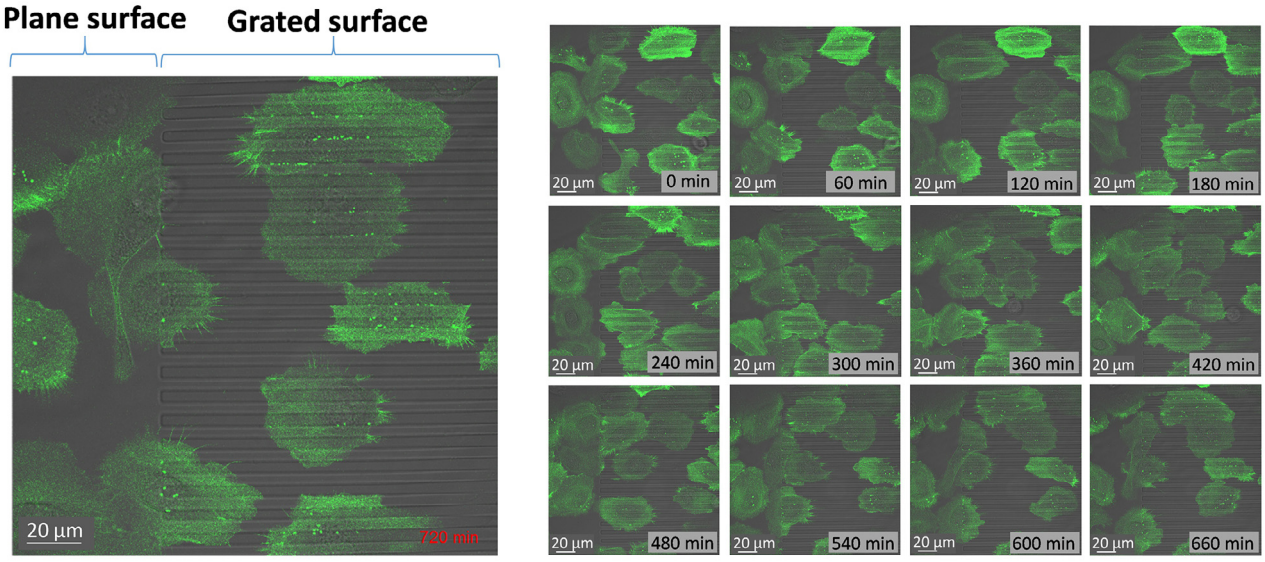

g

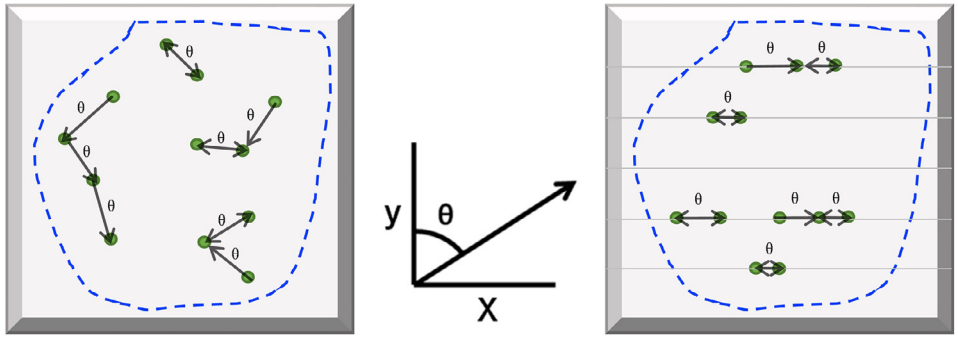

Perfect linear alignment between invadosomes: NNA θ= 90°

h

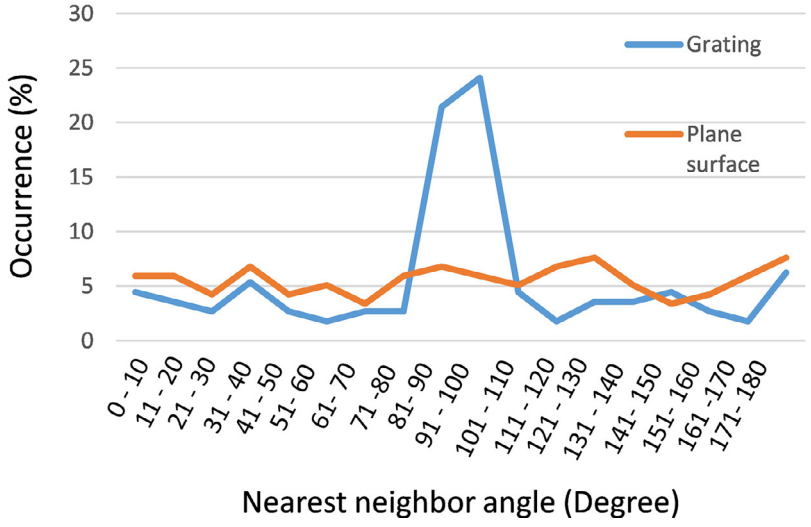

Fig. 3. Continued

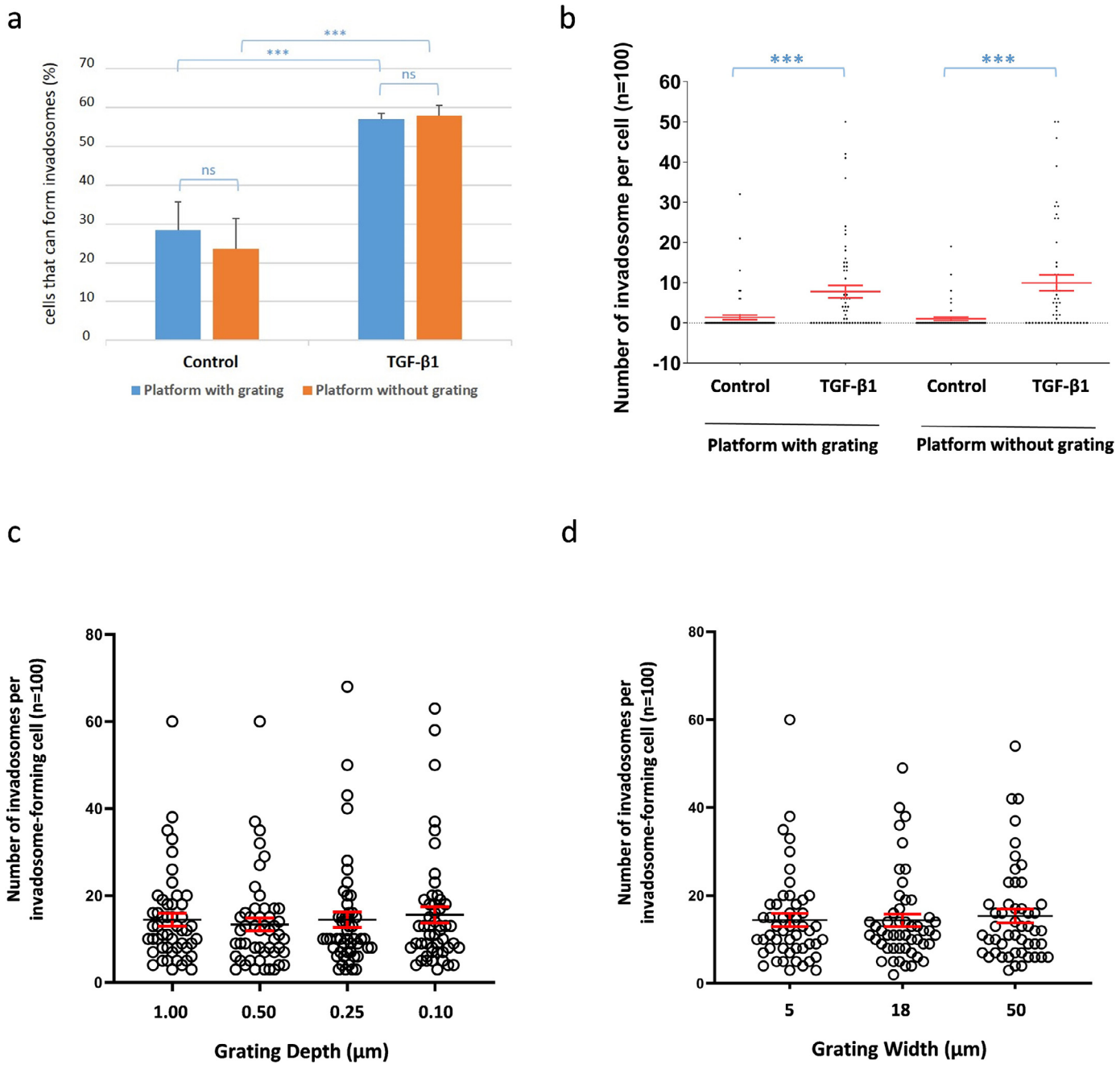

Fig. 4. 3D topography did not act as a stimulatory signal for invadosome formation. (a) The topographical gratings did not significantly alter the percentage of cells that can form invadosomes in control or TGF-β1-treated cells. (b) The number of invadosomes in control or TGF-β1-treated cells remained comparable on platform with or without grating. ***$p < 0.0005$ and ns: no significance. Under the treatment of TGF-β1, cells plated on platforms with different grating depths (c) and widths (d) have comparable number of invadosomes in each invadosome-forming cell.

TGF-β1-treated cells seeded on glass or PDMS surface, indicating the biomaterial for generating the gratings did not impose additional variables to the conventional invadosome assay in which cells are seeded on glass surface (Fig. 4b). Fig. 4c shows the number of invadosomes formed on patterns with different depths. In general, the total number of invadosome formed on platforms with different depths are comparable. In performing 2D invadosome assay, the cells were seeded on glass surface with a thin layer of gelatin coating. We have further counted the total number of invadosome formed by the cells when they were seeded on gratings with different widths. They formed similar number of invadosome on different grating widths. In fact, TGF-β1 is the factor that can upregulate the number of invadosome, while the topology of the platform affects the localization of the invadosome as shown in Fig. 4d.

3.4. Guidance of invadosome localization on edges is correlated with migration directionality on deep gratings

Our previous studies reported that gratings can guide cells to migrate along the grating [21,22]. Here we report the extent of guidance of invadosome location by the topographic pattern and also how it correlates with our previously reported directional guidance of cell migration. Fig. 5a shows the effects of grating depth on directionality of cell migration of NPC3 cells. One-way AVONA test was performed on cell migration angle on one-layer

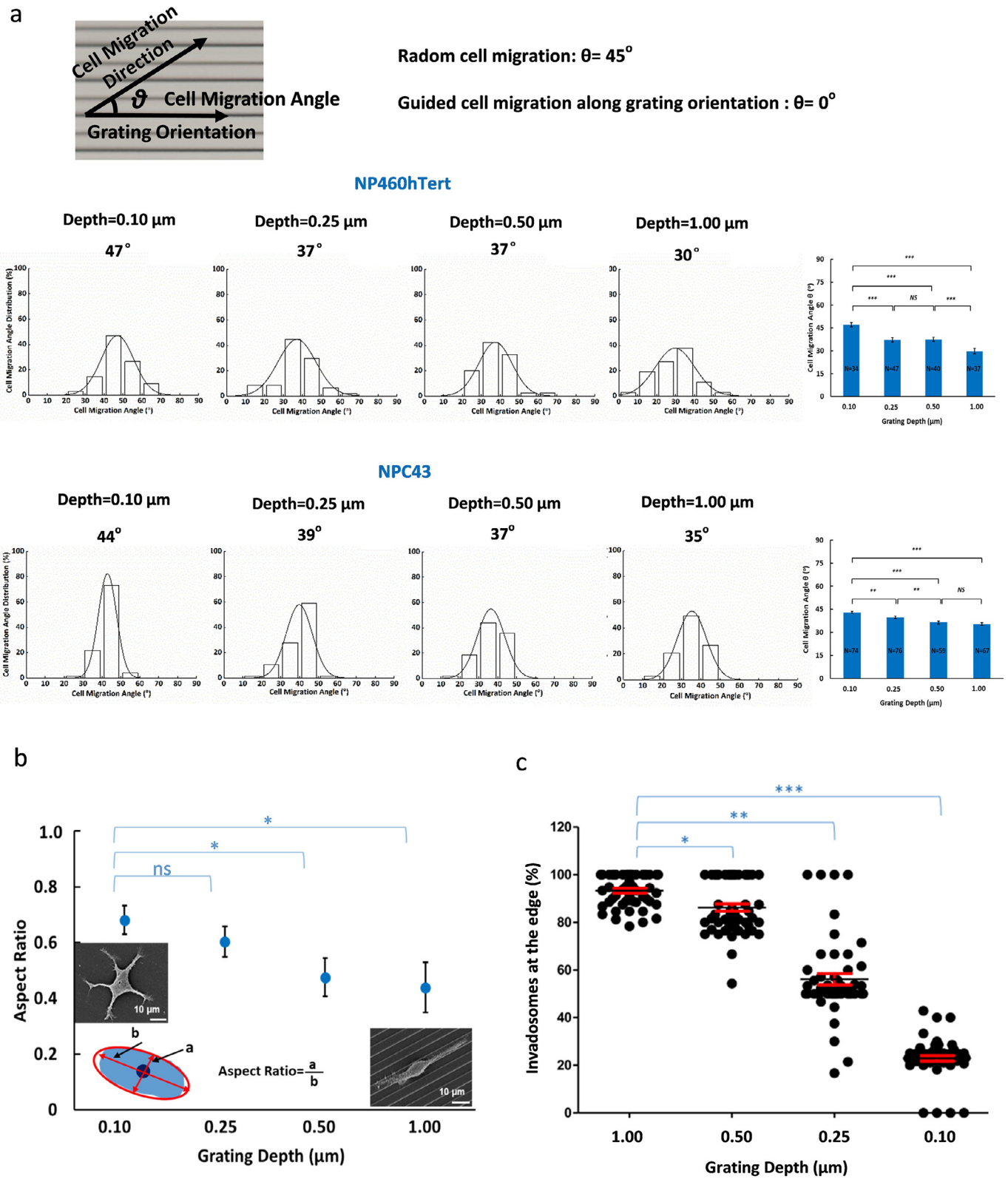

Fig. 5. Migration directionality on deep gratings was correlated with the localization of invadosomes at the edges. (a) Both NP460hTert and NPC43 were guided to migrate along the gratings when the grating depth increased from 0.10 to 1.00 μm. The width/space of the gratings were 5/5 μm and 10:1 PDMS was used for generating the platform. Cell migration angle [θ] between cell migration direction and grating orientation were measured. $n = 100$. The bar charts at the right panel show the statistic analysis (one-way AVNOA test) of cell migration angle of NP460 (upper chart) and NPC43 (lower chart) cells on the platforms with increased grating depth from 0.10 to 1.00 μm. (b) Effects of grating depth on the aspect ratio of minor and major axes for fitting ellipse around cell. (c) Nearly most invadosomes were guided to form along the edge of the ridges when the grating depth increased to 1 μm. $^{*}p < 0.05$, $^{**}p < 0.005$ and $^{***}p < 0.0005$.

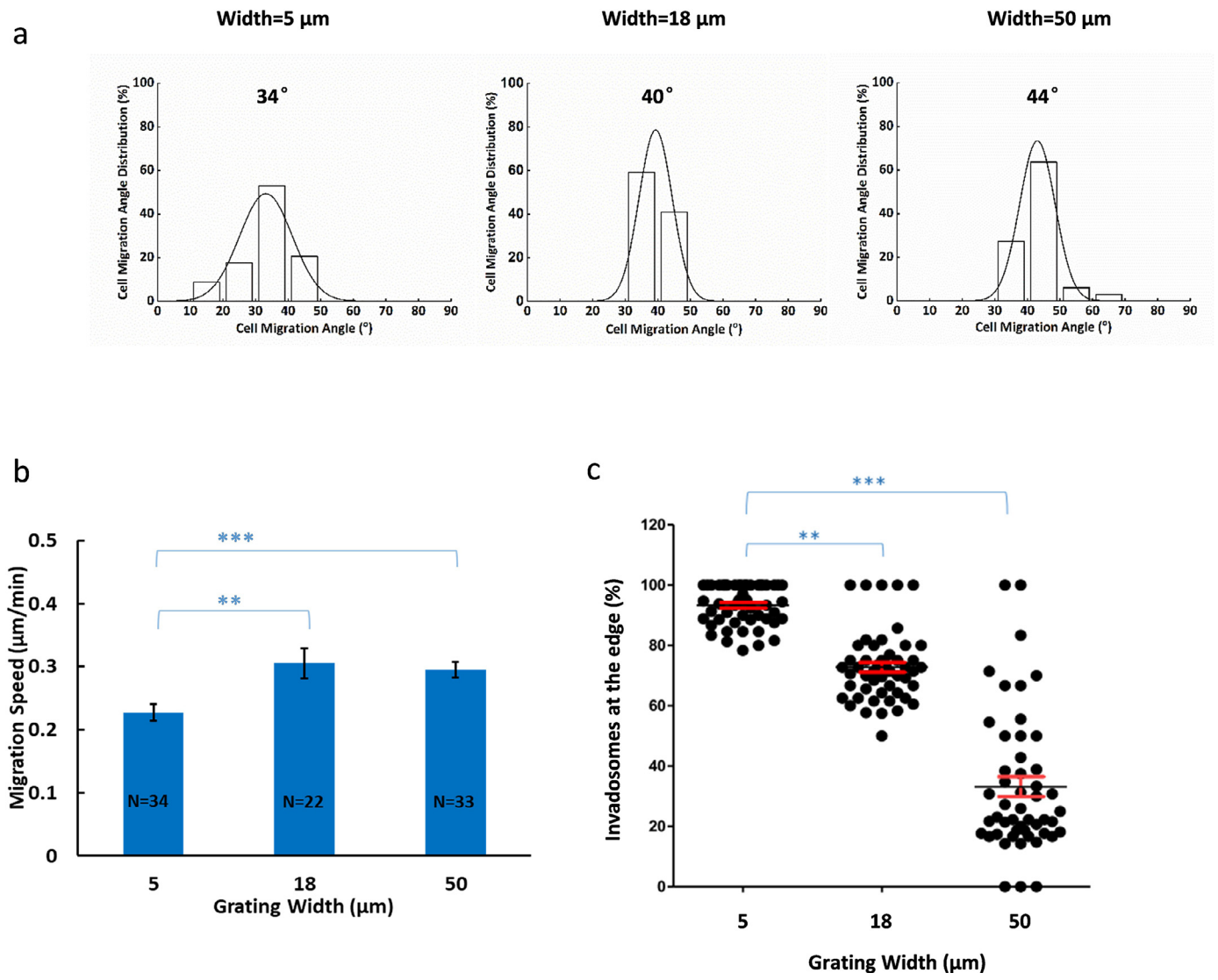

Fig. 6. Migration directionality on narrow gratings was correlated with the localization of invadosomes at the edges. (a) Nasopharyngeal cells were guided to migrate along the gratings when the grating width decreased from 50 to 5 μm. The depth of the gratings was 1 μm and 10:1 PDMS was used for generating the platform. Cell migration angle [θ] between cell migration direction and grating orientation were measured. $n = 100$. (b) Cells seeding on grating with a width of 5 μm migrated significantly slower than that of cells on grating with a width of 18 or 50 μm. (c) Nearly most invadosomes were guided to form along the edge of the ridges when the grating width decreased to 5 μm. $^{**}p < 0.005$ and $^{***}p < 0.0005$.

platforms with different grating depths from 0.10 to 1.00 μm. Both NP460 and NPC43 cells demonstrated a significant difference on cell migration angle changes with grating depth, showing cell migration was more directional on deeper platforms. Both NPC43 and NP460 cell migration became more directional as the grating depth increased from 0.10 to 1.00 μm. Thus, a grating depth of 0.10 μm was not as effective in guiding the cells along the edges of the gratings, while gratings with a depth of 0.25 to 1.00 μm was able to guide the cells along the grating orientation. Cell migration directionality was found to be related with cellular extensions into the trenches of gratings [10]. In this study, 0.10 and 0.25 μm deep gratings may provide less surface area in trenches for cells to form FAs compared to gratings with deeper trenches. The extent of forming FAs in the trenches may be reflected by the aspect ratio of NPC43 cells on platforms with different grating depths. From Fig. 5b, it can be seen that cells were more rounded on platforms with shallower gratings, and became more elongated on platforms with deeper gratings. Cells on 0.10 μm deep gratings exhibited a symmetrical star-like morphology and protrusions extended randomly in all directions. On 1.00 μm deep gratings, cells became more asymmetrical and the protrusions was elongated along the grating orientation. Thus, cells were not guided to move along the orientation of the ridges on shallower gratings that were less than 1 μm deep.

We also analysed the localization of invadosomes of 50 cells on each grating with different depth (Fig. 5c). In each cell, the percentage of invadosomes was calculated by 'number of invadosome on edge/total number of invadosomes X 100%'. We found that the guidance effect dropped from ~95% to ~25% when the depth of gratings was decreased from 1 μm to 0.1 μm (Fig. 5c). Taken together, the likelihood of invadosomes forming at the edges was correlated with the topographic control on cell migration directionality on deeper gratings. The number of invadosomes were comparable in TGF- β1-treated cells when they were either seeding on plane or grated surfaces, indicating the grating was not a stimulating factor for the formation of invadosomes. On the other hand, when the cells were seeded on grated surface, invadosomes were shown to be formed at edges of the grating. The

axial movement is guided by the topographical pattern of the parallel grating as reported previously [21,22,29]. The observation of linear alignment of invadosomes along the parallel gratings does not suggest that these protrusion can guide the cell migration direction.

3.5. Invadosomes preferentially form at edges when the cells move at a lower speed with guided directionality on narrow gratings

Next, we also investigated the role of grating width on the localization of invadosome to edges. Grating with width of 5, 18 and 50 μm and depth of 1 μm were fabricated. Fig. 6a shows that cell migration directionality decreased as the grating width increased from 5 to 50 μm with a depth of 1.00 μm. The cell migration guidance effect along the grating orientation was more effective for narrower grating width as they provided a higher density of grating edges for cell attachment. When the grating width was 5 μm, cells were better guided along the grating orientation. With 50 μm wide gratings, cells showed random migration direction. The rate of cell motility on gratings with different widths is also shown in Fig. 6b. The cell migration speed on 18 or 50 μm wide gratings was higher than gratings with 5 μm width. The results showed that the cells were more prone to move along the grating direction if the cells were seeded on grating patterns with higher density of ridges (*i.e.* with narrower ridges). The migration speed of the cells was also lower if the cells were seeded on higher density of ridges. The cell migration speed is related to the distribution of FAs near its leading and trailing regions. [21,22,29]. How the density of ridges affects the FA distributions remains to be elucidated. However, the FAs have a distinctive pattern that is different from that of invadosomes. While alignment of invadosomes along the ridges' edges was observed, the FAs (as visualized by mcherry-talin being stably expressed in NP460 cells) were found to be formed at the edge of the cell membrane as shown in Supplementary Figure S3.

The percentage of invadosomes on the edges of gratings was also calculated when the cells are seeded on grating with different width (Fig. 6c). Numbers dropped from ~90% to ~40% when the grating width increased from 5 to 50 μm. This suggests that when cells move slower and with efficient directionality along the gratings, they are more prone to form invadosomes at the edges.

3.6. Invadosomes formed at the edges have higher stability than those formed on plane surface

All previous experiments established an efficient guidance of invadosome forming on 3D topologic gratings with a minimal of 5 μm width and 1 μm depth. Interestingly, when we analyzed the stability of individual invadosomes as indicated by the appearance time between assembly and disassembly of each invadosome, the stability of invadosomes on the edges was significantly higher than those randomly formed on plane surfaces (Fig. 7). The number of invadosome was taken into account by counting the number of actin cores on top of black area, Figs. 1 and 2 indicate that TGF-β1 increases total active invadosome formation. For the effect of TGF- β1 in affecting the assembly and turnover of the invadosomes, analysis was performed by measuring the duration of each invadosome in untreated and TGF- β1-treated cells (Fig. 7b). TGF-β1 also enhanced the stability of the invadosomes.

3.7. Invadosome guidance is not affected by the substrate rigidity ranged from 1 to 8 MPa

Next, we aimed to investigate if stiffness of substrate may also affect the invadosome distribution on edges. By increasing the PDMS base:agent mix ratio from 5:1 to 30:1, the grating platforms became softer, ranged from 7.28 to 1 MPa. The localization of invadosomes of cells seeded on grating with 5 μm width and 1 μm depth was observed. In these range of substrate stiffness, there was no alteration in the efficiency of forming the invadosome on edges (Supplementary Figure S4).

4. Discussion

This study sought to understand the integration of biological and geometric signals for initiating the formation of invadosomes and their spatial regulation in invasive nasopharyngeal cells. NPC is a highly metastatic cancer with heavy infiltration of stromal cells [9]. The stromal cells including T-cell, B-cells and tumor-associated macrophages have been suggested to secret inflammatory cytokines for promoting invasive behavior of nasopharyngeal epithelial cells during NPC development. TGF-β1 was upregulated in NPC patients with higher relapse rate and metastatic potential [12,13]. Here, we firstly reported that TGF-β1 can promote the formation of invadosomes in nasopharyngeal cells (Fig. 1 and 2). It can act as an external molecular signal in inducing the formation of invadosomes. Once the cells are activated, invadosomes form randomly at the ventral cell membrane in contact with the substrate.

Moreover, *in vivo* settings, the formation of invadosomes may also be affected by the topographic changes caused by continuous or discontinuous ECM. The surfaces that cells encounter during migration can either be continuous ones where the dimension of any gap is negligible compared with cell size (for example, basement membranes) or discontinuous ones where the spacing between ECM fibres or cell junctions is greater than a few hundred nanometres (for example, collagen bundles and discontinuous cell-cell adhesion sites) [17]. In addition, micropatterning of linear collagen fibres was shown to guide the cells in the direction corresponding to the dimension of the substrate, a phenomenon known as contact guidance [30–32]. This observation mimics the phenomenon of cancer cells migrating out of tumours along linear collagen fibres [17,33]. Recent advances in microfabrication techniques have enabled us to generate biocompatible 3D platforms with defined micro- or nano-scale topography and rigidity that can mimic stromal environments [34]. Interdisciplinary technological advances thus provide us with an opportunity to understand the integrated roles of the biological factors and topographic changes during invasive movement and the regulation of the spatial distribution of invadosomes. In this study, we adopt techniques derived from optics and nanotechnology to elucidate the dynamics of invadosomes in live-imaging (Fig. 3). We demonstrated that nasopharyngeal cells respond to 3D topographic patterns by spatially aligning the invadosomes to the edges of ridged gratings.

This strongly suggests an integrated regulation of the physical-chemical properties of the microenvironment in which, on a 2D surface, invadosome formation can be promoted by TGF-β1 and/or its downstream intracellular signaling pathways. Most likely, intracellular components such as actin, invadosomal scaffold proteins and signaling molecules are now efficiently assembled to give rise to increased number of invadosomes per cell. When TGF-β1-activated cells were seeded on topographical platforms with different depth (1.00, 0.50, 0.25 and 0.10 μm) and width (5, 18 and 50 μm), we observed significant modulation of the localization of invadosomes (Fig. 5 and 6). Thus engineered platforms serve as *in vitro* microsystems to provide physical control on the guidance of invadosome formation of nasopharyngeal cells.

In this study, we found that TGF-β1-activated nasopharyngeal cells respond to 3D micropatterned substrates by aligning invadosomes at sites of high membrane curvature, *i.e.* at the edges of gratings. When the topographic disruptions reach a particular density (5 μm width and 1 μm depth), nearly all invadosomes will be

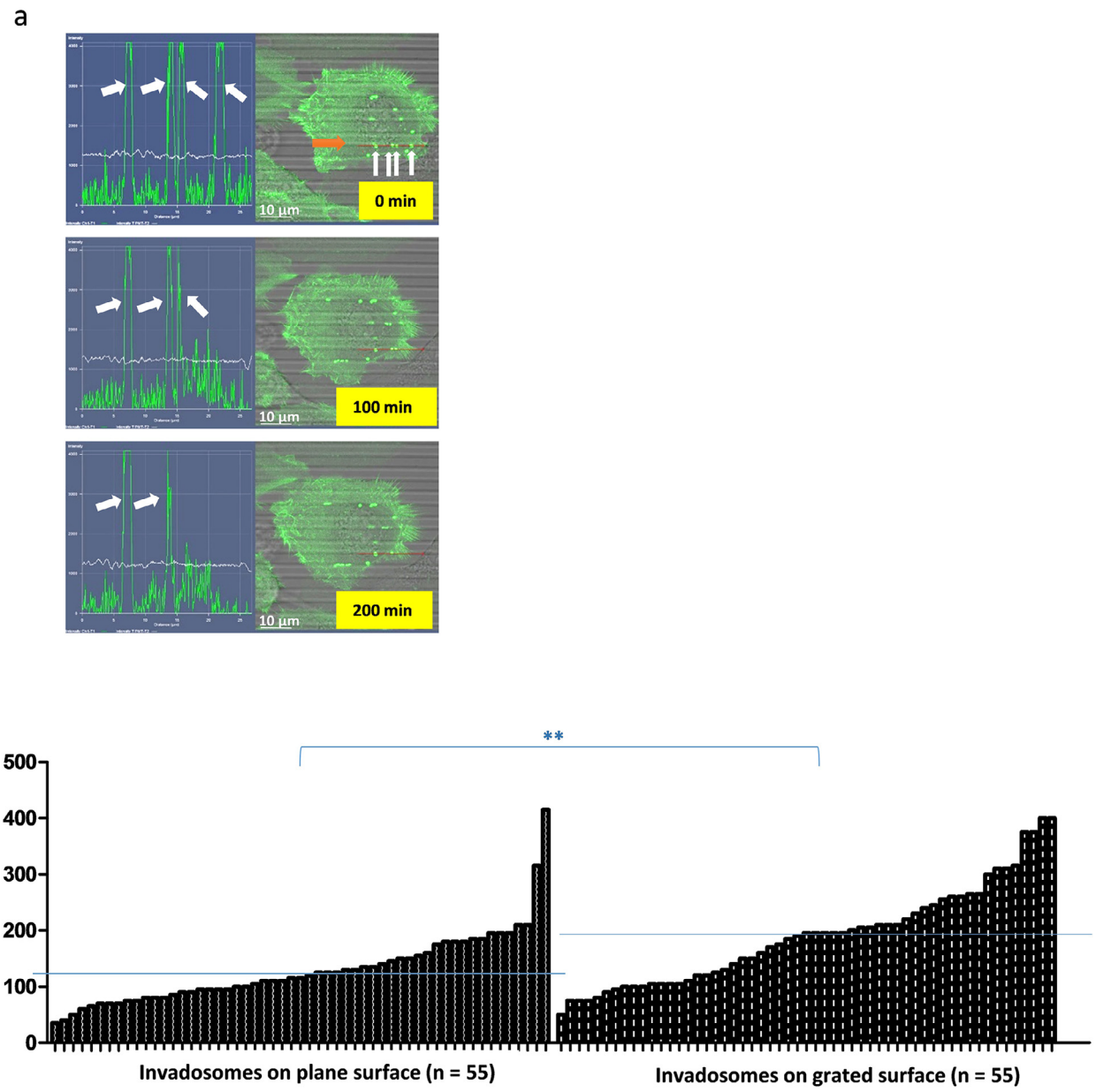

Fig. 7. The stability of invadosome was relatively higher when the TGF-beta3 treated cells were seeded on grated surface than on plane surface. (a) Analysis of the duration of invadosomes in control or TGF-β1-treated cells by Zen Imaging software. The left panel shows the fluorescence intensity along a designated edge as denoted by a red line on the cell in the right panel. The white arrows point to the fluorescence peaks which represent invadosomes. 2 out of four invadosomes dismissed within 200 mins. (b) The invadosomes formed by cells on grated surface had longer duration of appearance than the cells on plane surface. The period between the assembly and disassembly of each invadosome was recorded by live-cell imaging ($n = 55$). $^{**}p < 0.005$.

Summary: Nasopharyngeal epithelial cells are very sensitive to TGF-β1 for enhanced formation of invadosomes. TGF-β1 can promote the NP cells to form invadosomes at random places on plane surface. Nevertheless, the location of the invadosomes can be topographically guided to the edges. A grating platform of 1 μm depth and 5 μm width can efficiently direct nearly 100% of invadosomes to the edges.

localized along the edges (Fig. 5c and c). Importantly, even 100 nm depth of trench is sufficient to induce around 30% of invadosomes to from at the edged space (Fig. 5c). This suggests that nasopharyngeal cells, when invading in tissues, can sense the topology of individual ECM fibers or bundles, which vary in size between 30 and 300 nm, and concentrate invadosomes at hotspots of high curvature of the plasma membrane.

Previous reports have indicated that cells have evolved means to directly sense surface topology [17,35]. The surfaces that a cell encounters will influence the curvature of the plasma membrane. At the curved membrane region, BAR (Bin/Amphiphysin/Rvs) proteins may be preferentially accumulated as a result of their intrinsic crescent shape [36]. They also help to maintain membrane curvature by interacting with conical-shaped lipids (for example, phosphatidylinositol phosphates including PtdIns(4,5)P2). It is worth noting that PtdIns(4,5)P2 is the membranous lipid which initiate the actin nucleation for invadosome formation [37]. Therefore, it is possible that membrane curvature can passively accumulate the initiating factors for invadosomal protrusion [38]. This may also explain why the invadosomes forming at the edges have higher stability than the ones forming on plane surface, where the initiating factors may easily diffuse apart in the mosaic lipid bilayer of cell membrane (Fig. 7b). Although the precise utility of this mechanism is unclear, it might enable cells to drill through the matrix by locally increasing the concentration of MMP at crosslinked fibres or cell gaps.

We also observed that the accumulation and stability of invadosome along the edges was correlated with the migration directionality on the grated surface [21,22]. This may be explained by the tendency of cells to form more stable FAs along the trenches. Many cells adopt a polarized morphology when cultured on matrix ridges, with their long axis parallel to the ridges. This alignment can be induced by topological effects that prevent the efficient extension of linear or planar actin protrusions perpendicular to the ridges. It leads to elongation of the cell along the gratings and determines the direction of cell migration [17,21,22]. Cell migration on structured substrates composed of parallel ridges (0.4 – 4 μm in width and 0.2 – 0.4 μm in height) is reminiscent of that on fibrillar matrices. In the present study, gratings with 5 μm width and 1 μm depth induced cell migration directionality along the ridges, slowed down the cell migration speed, and guided most invadosomes to form at the edges (Fig. 5 and 6). It suggests that the cells moving along the gratings may help to maintain the preferential localization and stability of invadosomes at the matric gaps. This may also reflect an effective way of ECM degradation for invasive movement *in vivo*.

The physical deformability of the environment can vary by orders of magnitude between different tissues [39]. Rigidity is therefore another important factor to be taken into account when considering cell invasion [40]. Indeed, many cells can sense rigidity of the ECM in a process known as mechanotransduction and promote the activity of invadosomes [39]. In this study, the elastic modulus of the PDMS platforms ranged from 1 to 8 MPa which is similar to that of connective tissue. In this range of elastic modulus, no significant alteration in the invadosome guidance was observed (Supplementary Figure 2). However, stromal matrix sometimes exhibits a much lower elastic modulus. Future investigation is warranted by utilizing other biocompatible substrates which are much softer than PDMS. Moreover, substrate that allows the invasion of cells in all dimensions will enable better understanding of the cell behavior in 3D.

Another point worth to be discussed is the varied responses to biological and topographic cues of different cell types in the generation of invadosomes. In a study using hepatocellular cell (HCC) lines, TGF-β1 could not promote the invadosome formation [41]. However, when the cells were seeded on collagen-1 coated surface, the cells spontaneously formed lots of invadosomes with a linear alignment on the collagen fiber [41]. TGF-β1 was also shown to potentiate the collagen-1-induced formation of invadosomes [41]. In our study, TGF-β1 alone signals the induction of invadosome formation (Fig. 1and 2), whereas the topographic cues which may be resembled by the presence of collagen fibers cannot induce the formation of invadosomes (Fig. 4). Previous report has also demonstrated that dendritic cells could also form aligned invadosomes on ridges [23]. Interestingly, this 3D geometric guidance could prevent the dissociation of invadosomes under prostaglandin E2 (PGE2) [23]. The author suggested this behavior may be important for physiobiological functions of this type of immune cell. In our cell system, in contrast, the nasopharyngeal may take in the topographic cues to stabilize the formation of invadosomes in an inflammatory environment. To further understand the physiological functions of invadosomes, investigations on their spatial localization *in vivo* will be needed. Previous study has reported the visualization of invadosomes *in vivo* based on the presence of markers such as cortactin and Tks5 using high-resolution multiphoton microscopy of human breast carcinoma xenografts in SCID mice [5,42]. In future, it is worth to study if the formation of invadosomes of NPC cells would be correlated with a variety of microenvironmental factors, including the presence of cytokines and density of collagen fibers. In particular, it will be interestingly to observe whether the invadosomes are formed at spatially distinct regions of the tumor microenvironment such as near collagen fibers and blood vessels.

In this study, formation of degradative protrusion was observed in nasopharyngeal epithelial cell lines established by immortalization of premalignant nasopharyngeal tissues. The actin-rich cell surface structures with proteolytic activity on the nasopharyngeal cells are referred as invadosomes, which can be used to denote both the invadopodia and podosomes [15,43,44]. In general, invadopodia and podosomes are referred as the ECM-degrading membrane protrusions on tumor and normal cells, respectively. These protrusions may resemble more as 'invadopodia' which can provide the degradative properties to dysplastic nasopharyngeal epithelial cells and drive them to become highly invasive cancer cells under stimulations from *in vivo* microenvironment. We have also observed that the protrusions formed in the nasopharyngeal cells are long-lived and can last for hours (Fig. 7). This is also one of the major characteristics of invadopodia but not podosomes, which are very short-lived and can only last for a few minutes. However, we have not detected the expression of key regulatory proteins which can clearly distinguish the invadopodia from podosomes, such as Nck1 and Mena which are found in tumor cell invadopodia but not podosomes; or WASP and Grb2 which are found in podosomes but not invadopodia [15,45]. Future investigations are needed to define these protrusions as invadopodia through their structural and functional properties.

Gaining a full understanding of cell invasion and formation of invadosomes of a specific cell type under biomimetic *in vivo* environments is a formidable task. In this study, the biochemical induction of invadosome formation by TGF-β1 in nasopharyngeal cells was observed. Moreover, it is interesting to note that cells may be sensitive to topographical pattern accompanied with spatial re-organization of invadosomes. The invadosomes formed at the membrane curvatures also attain a higher stability than those formed on plane surface. In the future, careful molecular and mechanistic studies of biological and physical stimulations encountered by invasive cells may give insights on disrupting the functions of invadosomes for controlling the metastatic spread of cancer cells.

Declaration of Competing Interest

The authors declare that they have no known competing financial interests or personal relationships that could have appeared to influence the work reported in this paper.

Acknowledgements

This work was supported by the Center for Biosystems, Neuroscience, and Nanotechnology (CBNN) of City University of Hong Kong (9360148, 9380062); the University Grants Council of Hong Kong (GRF Projects: 17120814, 17110315, 11247716, and 11218017, 11213018) and CRF projects: C1013-15, C7027-16G; and the UK Medical Research Council (MR/K015664).

Data Availability

The raw and processed data required to reproduce these findings cannot be shared at this time due to technical or time limitations.

Supplementary materials

Supplementary material associated with this article can be found, in the online version, at doi:10.1016/j.actbio.2019.10.043.

References

[1] V.V. Artym, Y. Zhang, F. Seillier-Moiseiwitsch, K.M. Yamada, S.C. Mueller, Dynamic interactions of cortactin and membrane type 1 matrix metalloproteinase at invadopodia: defining the stages of invadopodia formation and function, Cancer Res. 66 (6) (2006) 3034–3043.

[2] J. Di Martino, E. Henriet, Z. Ezzoukhry, J.G. Goetz, V. Moreau, F. Saltel, The microenvironment controls invadosome plasticity, J. Cell Sci. 129 (9) (2016) 1759–1768.

[3] C.M. Gould, S.A. Courtneidge, Regulation of invadopodia by the tumor microenvironment, Cell Adh. Migr. 8 (3) (2014) 226–235.

[4] S. Linder, Invadosomes at a glance, J. Cell Sci. 122 (Pt 17) (2009) 3009–3013.

[5] B. Gligorijevic, J. Wyckoff, H. Yamaguchi, Y. Wang, E.T. Roussos, J. Condeelis, N-WASP-mediated invadopodium formation is involved in intravasation and lung metastasis of mammary tumors, J. Cell Sci. 125 (Pt 3) (2012) 724–734.

[6] H.S. Leong, A.E. Robertson, K. Stoletov, S.J. Leith, C.A. Chin, A.E. Chien, M.N. Hague, A. Ablack, K. Carmine-Simmen, V.A. McPherson, C.O. Postenka, E.A. Turley, S.A. Courtneidge, A.F. Chambers, J.D. Lewis, Invadopodia are required for cancer cell extravasation and are a therapeutic target for metastasis, Cell Rep. 8 (5) (2014) 1558–1570.

[7] A.W. Lee, W.T. Ng, Y.H. Chan, H. Sze, C. Chan, T.H. Lam, The battle against nasopharyngeal cancer, Radiother. Oncol. J. Eur. Soc. Therap. Radiol. Oncol. 104 (3) (2012) 272–278.

[8] S.W. Tsao, C.M. Tsang, K.F. To, K.W. Lo, The role of Epstein-Barr virus in epithelial malignancies, J. Pathol. 235 (2) (2015) 323–333.

[9] S.W. Tsao, C.M. Tsang, K.W. Lo, Epstein-Barr virus infection and nasopharyngeal carcinoma, Philos. Trans. R. Soc. Lond. B Biol. Sci. 372 (1732) (2017).

[10] J. Tsang, V.H. Lee, D.L. Kwong, Novel therapy for nasopharyngeal carcinoma–where are we, Oral Oncol. 50 (9) (2014) 798–801.

[11] R. Buccione, G. Caldieri, I. Ayala, Invadopodia: specialized tumor cell structures for the focal degradation of the extracellular matrix, Cancer Metastasis Rev. 28 (1–2) (2009) 137–149.

[12] S. Velapasamy, C.W. Dawson, L.S. Young, I.C. Paterson, L.F. Yap, The dynamic roles of TGF-beta signalling in EBV-Associated cancers, Cancers (Basel) 10 (8) (2018).

[13] J. Xu, J. Menezes, U. Prasad, A. Ahmad, Elevated serum levels of transforming growth factor beta1 in Epstein-Barr virus-associated nasopharyngeal carcinoma patients, Int. J. Cancer 84 (4) (1999) 396–399.

[14] S. Mandal, K.R. Johnson, M.J. Wheelock, TGF-beta induces formation of F-actin cores and matrix degradation in human breast cancer cells via distinct signaling pathways, Exp. Cell Res. 314 (19) (2008) 3478–3493.

[15] R.J. Eddy, M.D. Weidmann, V.P. Sharma, J.S. Condeelis, Tumor cell invadopodia: invasive protrusions that orchestrate metastasis, Trends Cell Biol. 27 (8) (2017) 595–607.

[16] C. Varon, F. Tatin, V. Moreau, E. Van Obberghen-Schilling, S. Fernandez-Sauze, E. Reuzeau, I. Kramer, E. Genot, Transforming growth factor beta induces rosettes of podosomes in primary aortic endothelial cells, Mol. Cell Biol. 26 (9) (2006) 3582–3594.

[17] G. Charras, E. Sahai, Physical influences of the extracellular environment on cell migration, Nat. Rev. Mol. Cell Biol. 15 (12) (2014) 813–824.

[18] B. Blouw, M. Patel, S. Iizuka, C. Abdullah, W.K. You, X. Huang, J.L. Li, B. Diaz, W.B. Stallcup, S.A. Courtneidge, The invadopodia scaffold protein TKS5 is required for the growth of human breast cancer cells *in vitro* and *in vivo*, PLoS ONE 10 (3) (2015) e0121003.

[19] E.J. Hagedorn, L.C. Kelley, K.M. Naegeli, Z. Wang, Q. Chi, D.R. Sherwood, ADF/cofilin promotes invadopodial membrane recycling during cell invasion *in vivo*, J. Cell Biol. 204 (7) (2014) 1209–1218.

[20] K.C. Williams, M.A. Cepeda, S. Javed, K. Searle, K.M. Parkins, A.V. Makela, A.M. Hamilton, S. Soukhtehzari, Y. Kim, A.B. Tuck, J.A. Ronald, P.J. Foster, A.F. Chambers, H.S. Leong, Invadopodia are chemosensing protrusions that guide cancer cell extravasation to promote brain tropism in metastasis, Oncogene 38 (19) (2019) 3598–3615.

[21] Q.Y. Tang, W.X. Qian, Y.H. Xu, S. Gopalakrishnan, J.Q. Wang, Y.W. Lam, S.W. Pang, Control of cell migration direction by inducing cell shape asymmetry with patterned topography, J. Biomed. Mater. Res. A 103 (7) (2015) 2383–2393.

[22] Q.Y. Tang, W.Y. Tong, J. Shi, P. Shi, Y.W. Lam, S.W. Pang, Influence of engineered surface on cell directionality and motility, Biofabrication 6 (1) (2014) 015011.

[23] K. van den, Dries, S.F. van Helden, J. te Riet, R. Diez-Ahedo, C. Manzo, M.M. Oud, F.N. van Leeuwen, R. Brock, M.F. Garcia-Parajo, A. Cambi, C.G. Figdor, Geometry sensing by dendritic cells dictates spatial organization and PGE(2)-induced dissolution of podosomes, Cell Mol. Life Sci. 69 (11) (2012) 1889–1901.

[24] F. Alonso, P. Spuul, T. Daubon, I. Kramer, E. Genot, Variations on the theme of podosomes: a matter of context, Biochim. Biophys. Acta Mol. Cell Res. 1866 (4) (2019) 545–553.

[25] W. Lin, Y.L. Yip, L. Jia, W. Deng, H. Zheng, W. Dai, J.M.Y. Ko, K.W. Lo, G.T.Y. Chung, K.Y. Yip, S.D. Lee, J.S. Kwan, J. Zhang, T. Liu, J.Y. Chan, D.L. Kwong, V.H. Lee, J.M. Nicholls, P. Busson, X. Liu, A.K.S. Chiang, K.F. Hui, H. Kwok, S.T. Cheung, Y.C. Cheung, C.K. Chan, B. Li, A.L. Cheung, P.M. Hau, Y. Zhou, C.M. Tsang, J. Middeldorp, H. Chen, M.L. Lung, S.W. Tsao, Establishment and characterization of new tumor xenografts and cancer cell lines from EBV-positive nasopharyngeal carcinoma, Nat. Commun. 9 (1) (2018) 4663.

[26] C.M. Tsang, Y.L. Yip, K.W. Lo, W. Deng, K.F. To, P.M. Hau, V.M. Lau, K. Takada, V.W. Lui, M.L. Lung, H. Chen, M. Zeng, J.M. Middeldorp, A.L. Cheung, S.W. Tsao, Cyclin D1 overexpression supports stable EBV infection in nasopharyngeal epithelial cells, Proc. Natl. Acad. Sci. U S A 109 (50) (2012) E3473–E3482.

[27] A.C. Humphries, M.P. Dodding, D.J. Barry, L.M. Collinson, C.H. Durkin, M. Way, Clathrin potentiates vaccinia-induced actin polymerization to facilitate viral spread, Cell Host Microbe 12 (3) (2012) 346–359.

[28] W.G. Jiang, A.J. Sanders, M. Katoh, H. Ungefroren, F. Gieseler, M. Prince, S.K. Thompson, M. Zollo, D. Spano, P. Dhawan, D. Sliva, P.R. Subbarayan, M. Sarkar, K. Honoki, H. Fujii, A.G. Georgakilas, A. Amedei, E. Niccolai, A. Amin, S.S. Ashraf, L. Ye, W.G. Helferich, X. Yang, C.S. Boosani, G. Guha, M.R. Ciriolo, K. Aquilano, S. Chen, A.S. Azmi, W.N. Keith, A. Bilsland, D. Bhakta, D. Halicka, S. Nowsheen, F. Pantano, D. Santini, Tissue invasion and metastasis: molecular, biological and clinical perspectives, Semin. Cancer Biol. 35 (2015) S244–S275 Suppl.

[29] S.F. Zhou, S. Gopalakrishnan, Y.H. Xu, J. Yang, Y.W. Lam, S.W. Pang, A unidirectional cell switching gate by engineering grating length and bending angle, PLoS ONE 11 (1) (2016) e0147801.

[30] P.P. Provenzano, K.W. Eliceiri, J.M. Campbell, D.R. Inman, J.G. White, P.J. Keely, Collagen reorganization at the tumor-stromal interface facilitates local invasion, BMC Med. 4 (1) (2006) 38.

[31] A. Ray, O. Lee, Z. Win, R.M. Edwards, P.W. Alford, D.H. Kim, P.P. Provenzano, Anisotropic forces from spatially constrained focal adhesions mediate contact guidance directed cell migration, Nat. Commun. 8 (2017) 14923.

[32] D.H. Kim, A.J. Ewald, J. Park, M.Kwak Kshitiz, R.S. Gray, C.Y. Su, J. Seo, S.S. An, A. Levchenko, Biomechanical interplay between anisotropic re-organization of cells and the surrounding matrix underlies transition to invasive cancer spread, Sci. Rep. 8 (1) (2018) 14210.

[33] V.P. Sharma, B.T. Beaty, A. Patsialou, H. Liu, M. Clarke, D. Cox, J.S. Condeelis, R.J. Eddy, Reconstitution of *in vivo* macrophage-tumor cell pairing and streaming motility on one-dimensional micro-patterned substrates, Intravital 1 (1) (2012) 77–85.

[34] D.H. Kim, P.P. Provenzano, C.L. Smith, A. Levchenko, Matrix nanotopography as a regulator of cell function, J. Cell Biol. 197 (3) (2012) 351–360.

[35] C. Mim, V.M. Unger, Membrane curvature and its generation by bar proteins, Trends Biochem. Sci. 37 (12) (2012) 526–533.

[36] H.T. McMahon, E. Boucrot, Membrane curvature at a glance, J. Cell Sci. 128 (6) (2015) 1065–1070.

[37] C. Albiges-Rizo, O. Destaing, B. Fourcade, E. Planus, M.R. Block, Actin machinery and mechanosensitivity in invadopodia, podosomes and focal adhesions, J. Cell Sci. 122 (Pt 17) (2009) 3037–3049.

[38] Z. Wu, M. Su, C. Tong, M. Wu, J. Liu, Membrane shape-mediated wave propagation of cortical protein dynamics, Nat. Commun. 9 (1) (2018) 136.

[39] N.R. Alexander, K.M. Branch, A. Parekh, E.S. Clark, I.C. Iwueke, S.A. Guelcher, A.M. Weaver, Extracellular matrix rigidity promotes invadopodia activity, Curr. Biol. 18 (17) (2008) 1295–1299.

[40] M.H. Zaman, L.M. Trapani, A.L. Sieminski, D. Mackellar, H. Gong, R.D. Kamm, A. Wells, D.A. Lauffenburger, P. Matsudaira, Migration of tumor cells in 3D matrices is governed by matrix stiffness along with cell-matrix adhesion and proteolysis, Proc. Natl. Acad. Sci. U S A 103 (29) (2006) 10889–10894.

[41] Z. Ezzoukhry, E. Henriet, L. Piquet, K. Boye, P. Bioulac-Sage, C. Balabaud, G. Couchy, J. Zucman-Rossi, V. Moreau, F. Saltel, TGF-beta1 promotes linear invadosome formation in hepatocellular carcinoma cells, through DDR1 up-regulation and collagen I cross-linking, Eur. J. Cell Biol. 95 (11) (2016) 503–512.

[42] E. Genot, B. Gligorijevic, Invadosomes in their natural habitat, Eur. J. Cell Biol. 93 (10–12) (2014) 367–379.

[43] S. Linder, C. Wiesner, M. Himmel, Degrading devices: invadosomes in proteolytic cell invasion, Annu. Rev. Cell Dev. Biol. 27 (2011) 185–211.

[44] A. Parekh, A.M. Weaver, Regulation of invadopodia by mechanical signaling, Exp. Cell Res. 343 (1) (2016) 89–95.

[45] M. Oser, A. Dovas, D. Cox, J. Condeelis, Nck1 and GRB2 localization patterns can distinguish invadopodia from podosomes, Eur. J. Cell Biol. 90 (2–3) (2011) 181–188.